radiation

MDPI

Article

On the Monte Carlo Calculation of the Air-Kerma Strength for Brachytherapy Sources

Rafael Guerrero [1,2], Julio F. Almansa [2,3] and Antonio M. Lallena [2,4,*]

[1] Unidad de Radiofísica, Hospital Universitario Clínico "San Cecilio", E-18016 Granada, Spain; rafael.guerrero.alcalde.sspa@juntadeandalucia.es
[2] Instituto de Investigación Biosanitaria (ibs.GRANADA), Complejo Hospitalario Universitario de Granada, Universidad de Granada, E-18016 Granada, Spain; juliof.almansa.sspa@juntadeandalucia.es
[3] Servicio de Radiofísica y P.R., Hospital Universitario "Virgen de las Nieves", E-18014 Granada, Spain
[4] Departamento de Física Atómica, Molecular y Nuclear, Universidad de Granada, E-18071 Granada, Spain
* Correspondence: lallena@ugr.es

Simple Summary

Monte Carlo calculation of air-kerma strength for high dose-rate sources is studied. Some of the effects are relatively large in both ^{192}Ir and ^{60}Co sources. Electrons produce significant contributions to air-kerma strength and using μ_{en} instead of μ_{tr} reduces it significantly. Fluence bin size may modify the air-kerma strength up to 0.5%. Overall effects of up to 1% may occur in the calculation of the air-kerma strength.

Abstract

Purpose: To study in detail how the various quantities entering the calculation of the air-kerma strength of brachytherapy sources affect the final value of this key quantity. Specifically, this study examines the role of the electrons emitted by the β radioisotopes used in brachytherapy sources, the effect of using μ_{en}/ρ instead of μ_{tr}/ρ, how the size of the bin used to determine the detected photon fluence modifies the final value of the air-kerma strength, the dependence of this value on the considered threshold photon energy, and how the level of detail with which simulations are carried out may affect the results of the calculations. *Methods*: Using the Monte Carlo code PENELOPE, the air-kerma strength S_K is calculated according to TG-43U1 protocol. Various simulations with different detail levels, electron transport parameters, and cut-off energies are conducted in order to elucidate how the various ingredients entering the definition of S_K affect its final value. Calculations are carried out for two sources: the ^{60}Co Flexisource Co-60 HDR and the ^{192}Ir microSelectron mHDR-v2r. *Results*: Fully neglecting electron production and transport modified S_K by 0.10% (2.0σ) for the Flexisource Co-60 HDR and 0.29% (14.1σ) for the microSelectron mHDR-v2r. The effect was larger in the case of the latter because electrons emitted by ^{192}Ir are on average more energetic than those emitted by ^{60}Co. Other ingredients of the calculation produced changes of the same order or bigger. For example, substituting μ_{tr}/ρ by μ_{en}/ρ reduced S_K by 0.39% (7.9σ) and 0.08% (3.9σ) for the Flexisource and microSelectron, respectively. Increasing the size of the energy bins employed to score the photon fluence rate from 1 keV to 10 keV increased S_K by 0.22% (4.4σ) for the Flexisource, while for the microSelectron a reduction of 0.49% (23.6σ) was obtained. Air composition also plays a role, producing changes of up to 0.16% when considering 40% moist air instead of dry air; a similar effect of up to 0.10% was generated by changing the low-energy photon threshold used to calculate the air-kerma rate. Finally, no differences significant within 1.7σ were found when using fully detailed or mixed electron transport schemes to carry out the simulations. *Conclusions*: Though electrons may seem not to affect kerma calculated via Monte Carlo simulation in an overall analysis of the problem, the more detailed study of

Check for updates

Academic Editor: Gabriele Multhoff

Received: 27 August 2026
Revised: 13 October 2026
Accepted: 14 October 2026
Published: 19 October 2026

Copyright: © 2026 by the authors. Licensee MDPI, Basel, Switzerland. This article is an open access article distributed under the terms and conditions of the Creative Commons Attribution (CC BY) license.

their role carried out in the present work indicates that they can produce significant effects in the obtained air-kerma strength that cannot be neglected. Other ingredients must also be considered, as their contributions to air-kerma strength may sum up to produce an overall effect of ∼1%.

Keywords: kerma; brachytherapy sources; TG-43U1; Monte Carlo; PENELOPE; electron effect

1. Introduction

The TG-43 protocol for dosimetric characterization of brachytherapy sources [1] and its TG-43U1 update [2] define the air-kerma ("kerma" stands for kinetic energy released per unit mass) strength as

$$S_K = \dot{K}_\delta^{\mathrm{ref}} \cdot d^2 \,, \tag{1}$$

where $\dot{K}_\delta^{\mathrm{ref}}$ represents the air-kerma rate in vacuum due to photons with energy greater than δ at a reference point located in the plane perpendicular to the source axis passing through its geometric center and at a distance d from this source center. It is recommended that d be 1 m, a distance sufficiently large compared to the dimensions of the source, which allows for the assumption that the source behaves as a point source. Here, "in vacuum" means that after measuring the air-kerma rate, it must be corrected to account for the effects of the air (photon attenuation and scattering) or any other medium present between the source and the detector as well as for any objects (walls, floors, or ceilings) surrounding the source. Furthermore, the energy limit δ permits ignoring contributions from low-energy photons originating from the source metal coating, which are not relevant to the dose at distances greater than a few millimeters from the source when it is immersed in water or tissue, as is the case in clinical practice. A value of $\delta = 5$ keV is typically adopted for sources that emit low-energy photons; for medium and high energies, which are those of interest in the present work, the HEBD-WG report recommends $\delta = 10$ keV [3,4].

To avoid many of the difficulties that arise when trying to measure the air-kerma rate, it can be calculated based on an appropriate configuration. Assuming that the z-axis coincides with the axis of symmetry of the source along its length, the air-kerma rate in vacuum at a point within air with polar coordinates (d, θ) is given by [5]:

$$\dot{K}_\delta(d,\theta) = \int_\delta^{E_{\max}} \mathrm{d}E \, \frac{\mu_{\mathrm{tr}}(E)}{\rho} \, E \, \dot{\Phi}_E(d,\theta) \,, \tag{2}$$

where E denotes the photon energy, $E_{\max}$ refers to the maximum energy of the emitted photons, $\mu_{\mathrm{tr}}(E)/\rho$ is the mass energy transfer coefficient for air (with μ_{tr} the energy transfer coefficient for air and ρ the air density), and $\dot{\Phi}_E(d,\theta)$ is the fluence rate of photons with energy E exiting the source. It is worth noting that this expression for the air-kerma rate as a function of the fluence rate permits dealing with the kerma rate for a given material at a point within a different material, in our case,

$$\dot{K}_\delta^{\mathrm{ref}} = \int_\delta^{E_{\max}} \mathrm{d}E \, \frac{\mu_{\mathrm{tr}}(E)}{\rho} \, E \, \dot{\Phi}_E^{\mathrm{ref}} \,, \tag{3}$$

where $\dot{\Phi}_E^{\mathrm{ref}} \equiv \dot{\Phi}_E(d = 1\,\mathrm{m}, \theta = 90°)$ is the fluence rate under reference conditions.

An approach that has been extensively used in this context is the Monte Carlo estimation of $\dot{K}_\delta(d,\theta)$. The procedure assumes that the source is in vacuum, surrounded by a very thin (a few microns) spherical shell filled with air and having an inner radius of 1 m. In the simulation, the spectrum of the photons arriving to the shell is scored to determine the corresponding photon fluence rate at the point of interest, $\dot{\Phi}_E(d,\theta)$. This is the approach used by Almansa et al. [6,7], Borg and Rogers [8], Guerrero et al. [9],

Taylor and Rogers [10,11] and Safigholi et al. [12]. Another way to calculate air-kerma rate uses the dose distribution due to the source when it is embedded in air, which is then corrected for the air effects. This second approach was considered in works by Ballester et al. [13], Daskalov et al. [14], Granero et al. [15] and Vijande et al. [16].

However, and independently of which approach is considered, these Monte Carlo estimations include several approximations applied to simplify the simulations. The first of these relates to the calculation of the photon fluence rate, where a common practice has been to perform simulations that neglect the electrons emitted by the radioisotopes present in the source (usually β emitters). In fact, the only mention of electrons in TG-43U1 refers to secondary electrons produced in the interactions of the photons emitted by the radionuclides, and establishes that no electron transport is required.

In the case of medium- and high-energy brachytherapy sources with high dose rate (HDR), in particular those containing ^{192}Ir and ^{60}Co radioisotopes, the electrons emitted in the decay process may have energies of up to 1.45 MeV and 2.82 MeV, respectively. It has been argued [13,17,18] that the electrons emitted in the beta decay of these sources, as well as those coming from internal conversion and Auger emissions, are absorbed practically within the source core and encapsulation, eventually contributing less than 1% to the total dose in water at distances very close to the source. On the other hand, Safigholi et al. [12] mentioned that transport of electrons in the sources can be neglected because air-kerma measurements are carried out using ionization chambers that respond only to photon fluences. However, TG-43U1 [2] highlights the need to account for the characteristic X-rays that may be produced following photoelectric absorption in atoms with medium or high atomic number, particularly in sources containing Ag or Pd. Despite this, no quantitative evaluation of the overall electron effects on S_K can be found in the literature.

Another commonly used approximation is that when the fraction of energy lost by charged particles through radiative processes is negligible, the mass energy transfer coefficient appearing in Equation (2) can be approximated by the mass energy absorption coefficient, which is tabulated in various sources (see, e.g., the NIST database [19]).

In the present work, Monte Carlo estimation of S_K is studied in detail, investigating the influence of including the beta emission spectra of the sources and the electron transport. Calculations are carried out using the Monte Carlo code PENELOPE-2024 [20] for two HDR sources: the ^{192}Ir microSelectron mHDR-v2r and the ^{60}Co Flexisource Co-60 HDR. In particular, we analyze the effects of the transport parameters used in the simulations. Another aspect we study is the change produced in S_K when it is calculated using the mass energy transfer coefficients, as indicated in Equation (2), instead of the mass energy absorption coefficients, as usually considered. In connection with this point, the influence of the energy bin size used to score the photon fluence rates is analyzed as well. When the beta emission spectrum of ^{60}Co is not included in the case of the Flexisource Co-60 HDR, we study the impact of using a complete photon emission spectrum, as recommended in [3,4], instead of a minimum photon emission spectrum containing only the two most probable photon emissions. Finally, in view of HEBD-WG [4] recommending dry air while TG-43 [1] and TG-43U1 [2] both recommend moist air, we analyze the influence of air composition.

2. Materials and Methods

2.1. HDR Sources

In this work, the air-kerma strength S_K is calculated for two HDR sources. Their schemes are drawn in Figure 1.

The first source is the Flexisource Co-60 HDR (Elekta, Stockholm, Sweden). The radioisotope is ^{60}Co; it is distributed uniformly within a cylinder made of pure Co, with a diameter of 0.5 mm and a height of 3.5 mm. The simulation geometry shown in Figure 1

is the same used in previous works [7,16,21]. In the following, this source is referred to as "Flexisource".

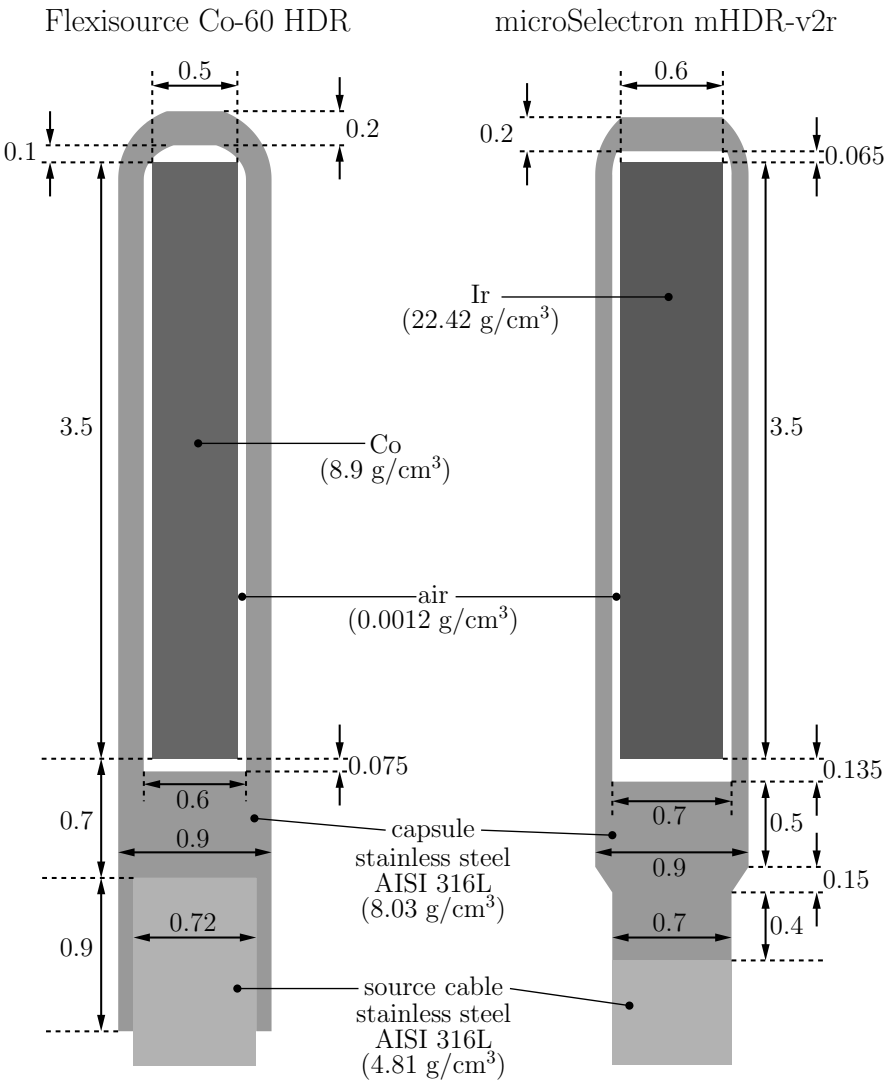


Figure 1. Schemes of the geometry of the Flexisource Co-60 HDR and the microSelectron mHDR-v2r sources studied in the present work. Dimensions are in mm. The stoichiometric composition (weight fraction) considered for AISI 316L was C (0.03%), N (0.1%), Si (0.75%), P (0.045%), S (0.03%), Cr (17%), Mn (2%), Fe (65.545%), Ni (12%), and Mo (2.5%). See Table 1 for air characteristics.

Table 1. Air stoichiometric compositions (as weight fractions in percentage) used in our simulations. PENELOPE dry air data correspond to material #104 in the database of the Monte Carlo code. TG-43U1 dry and moist (40%) air data are taken from [2].

	Dry Air		Moist Air (40%)
Element	**PENELOPE**	**TG-43U1**	**TG-43U1**
H			0.073
C	0.012	0.012	0.012
N	75.528	75.527	75.033
O	23.177	23.178	23.608
Ar	1.283	1.283	1.274
density ($g\,cm^{-3}$)	1.20479×10^{-3}	1.2×10^{-3}	1.2×10^{-3}

The second source is the microSelectron mHDR-v2r source (Elekta, Stockholm, Sweden), which incorporates ^{192}Ir as radioisotope embedded uniformly in an Ir cylindric core with a diameter of 0.6 mm and a height of 3.5 mm. In Figure 1, the complete source geometry used in the simulations is sketched. This geometry is the same as that used by other authors [6,12,15]. In the following, this source is denoted as "microSelectron".

2.2. Calculation of S_K

The calculation of S_K was carried out using Equation (1); to evaluate the air-kerma rate, the integral in Equation (2) was discretized as follows:

$$\dot{K}_\delta(d,\theta) \;=\; b_E \sum_{i=1}^{N} \frac{\mu_{\rm tr}(E_i)}{\rho}\, E_i\, \dot{\Phi}_{E_i}(d,\theta)\, \Theta(E_i-\delta)\,, \tag{4}$$

where $b_E = E_{\rm max}/N$ is the size of each of the N energy bins in which the photon energy interval has been divided, E_i is the central energy of the i-th bin, and $\Theta(x)$ is the Heaviside function, which takes a value of 0 when $x < 0$ or 1 when $x \geq 0$.

In the simulations carried out to estimate the photon fluence rates $\dot{\Phi}_{E_i}(d,\theta)$, the source was in vacuum in the center of a spherical 10 μm thick shell, with an inner radius of 1 m, filled with air and acting as a photon detector spectrometer. The calculations were carried out using the Monte Carlo code PENELOPE-2024 [20], which allows for simulation of the interactions of electrons, positrons, and photons with matter for energies ranging from 50 eV to 1 GeV. Photons are simulated in detail, and photon interactions are simulated one-by-one. Electrons and positrons are simulated within a mixed scheme in which collisions can be hard or soft depending on whether the polar deviation angles and/or energy losses are above or below certain specific threshold values set by the user. While hard events are simulated in detail, all soft interactions occurring between any two consecutive hard events are simulated as a single virtual event called a "hinge" using a multiple scattering approximation.

Electron and positron simulation is driven by several user-defined transport parameters. These parameters are as follows: C_1 and C_2 respectively refer to the average angular deflection and the maximum average fractional energy loss due to all soft interactions between two consecutive hard elastic events; $W_{\rm CC}$ and $W_{\rm CR}$ respectively fix the cut-off energies for hard inelastic collisions and hard bremsstrahlung emission; $E_{\rm abs}$ refers to the absorption energies in each material present in the simulation geometry for photons, electrons, and positrons, which establishes the energy thresholds below which simulation of the corresponding particle is stopped and its remaining energy is deposited locally; finally, $s_{\rm max}$ defines the maximum step between two successive interactions, which is strongly relevant when the simulation geometry includes very thin elements, as is the case with the sources simulated in this work. Users must choose the values of these parameters for each material present in the simulation geometry.

It is worth pointing out that if $C_1 = C_2 = W_{\rm CC} = 0$ and $W_{\rm CR} < 0$ are chosen, the simulation of electrons becomes fully detailed. The use of the transport parameters as well as their optimal values are described in the PENELOPE user manual [20].

In this work, PENMAIN, included in the PENELOPE distribution, was the main program employed to control the simulation process.

The air-kerma strength values obtained according to Equation (1), with $\dot{K}_\delta$ given by Equation (2), are labeled as $S_K^{\rm tr}$. When the mass energy absorption coefficient $\mu_{\rm en}/\rho$ is considered instead of the mass energy transfer coefficient $\mu_{\rm tr}/\rho$, as assumed in many previous studies [6–11], the obtained air-kerma strengths are instead labeled as $S_K^{\rm en}$.

Two sets of data were considered to find the values of these mass coefficients. The first was provided by the code MUTREN, included in the PENELOPE distribution. The values obtained for both $\mu_{\rm tr}/\rho$ and $\mu_{\rm en}/\rho$ in this way are fully consistent with the calculations of the fluence

rates. Different air compositions were also considered to determine the mass coefficients; Table 1 shows these compositions. In the following sections, unless otherwise indicated, the calculations are performed assuming TG-43U1 dry air.

A second set of data was taken from the NIST database [19]. In this case, a cubic spline interpolation was carried out to obtain the values required for the photon energies according to the bin sizes of the fluence rates.

2.3. Simulations

Depending on the emission spectra under consideration, three types of simulations were carried out. In the first, we used the complete disintegration schemes of ^{60}Co and ^{192}Ir as given in the NUCLEIDE database [22]. These emission spectra include all electrons (β, internal conversion and Auger) and photons (gamma and characteristic X-rays) emitted by the isotopes. These simulations, in which the full decay schemes of the isotopes were used, are labeled as `fuldec`.

In a second type of simulations, electrons were neglected; in these simulations, we considered all photon emissions included in the complete photon spectrum recommended in the HEBD-WG report [4]. These are labeled as `comphs`. The energies of the photon emissions considered in these simulations and their intensities are plotted in Figure 2 and listed in Tables A1 and A2 (see Appendix A).

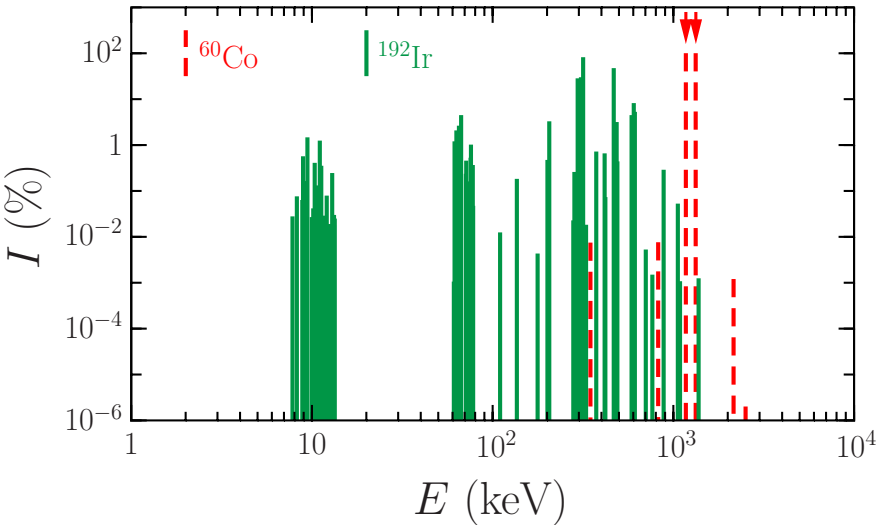


Figure 2. Intensities, I (in %) of the photon emissions considered in the `comphs` simulations as a function of their energies E; green solid lines correspond to ^{192}Ir and red dashed lines to ^{60}Co. These are the spectra recommended in the HEBD-WG report [4]. In the case of ^{60}Co, `minphs` simulations were also carried out by considering the two emissions marked with an arrow.

In the case of the Flexisource, a spectrum including only the two main photon emissions (those with energies 1173.23 keV and 1332.49 keV, indicated with arrows in Figure 2) was also considered. The corresponding simulations performed with this minimum photon spectrum are labeled as `minphs`.

We also studied the effect of the detail with which electron transport was modeled. In this case, results that were obtained in a fully detailed simulation (see above) were compared to those from mixed simulations in which $C_1 = C_2 = 0.05$, $W_{CC} = 10$ keV, and $W_{CR} = 1$ keV. These latter values are more restrictive than those recommended for "safe" simulations in the PENELOPE manual [20]. The corresponding results are labeled as "`det`" and "`mix`", respectively.

When referring to the absorption energies of electrons and positrons, $E_{abs}(e^{\mp}) = 100$ eV was used for all materials in all simulations except those where electron transport was not

simulated, in which case $E_{abs}(e^{\mp}) = 10\,\text{MeV}$. For photons, $E_{abs}(\gamma) = 1\,\text{keV}$ was used for all materials.

The s_{max} parameter was chosen as one tenth of the characteristic thickness of each component of the sources: 60 µm for the active core, 5 µm for the air separating the active core from the capsule, 10 µm for the capsule, and 90 µm for the cable.

Finally, photon spectra at the detection sphere were scored for energies up to 2 MeV. No photons with higher energies were detected. To analyze the effects linked to the size of the bins considered in Equation (4) for calculation of the integral defining the air-kerma rate, fluence spectra with bin sizes $b_E = 10\,\text{keV}$ (scored spectra with 200 bins) and $b_E = 1\,\text{keV}$ (scored spectra with 2000 bins) were calculated.

The number of histories to be followed was chosen according to the bin size of the scored photon spectra. Specifically, 10^9 histories were followed in all simulations performed with a fluence bin size of 10 keV, while 10^{10} were followed for 1 keV fluence bins. Throughout the text, type A uncertainties of the Monte Carlo results are shown with a coverage factor $k = 3$. They are given as a value between parentheses affecting the last significant figures.

The air-kerma strength unit employed in the present work was $1\,\text{U} = 1\,\text{GBq}^{-1}$, where $1\,\text{U} = 1\,\text{cGy}\,\text{cm}^2\,\text{h}^{-1}$.

Quantification of the studied effects was carried out by comparing S_K^{ref}, the air-kerma strength obtained in the reference simulation, and the corresponding S_K calculated in a simulation in which the model characteristic or property producing the effect of interest was neglected. Table A3 summarizes the characteristics of the various simulations in the present work. The reference simulation consisted of a `mix`, `fuldec` simulation that considered μ_{tr} in Equation (3) as obtained from the PENELOPE database while assuming the TG-43U1 dry air composition, an absorption energy for photons of $E_{abs}(\gamma) = 1\,\text{keV}$, an absorption energy for electrons and positrons of $E_{abs}(e^{\mp}) = 100\,\text{eV}$, a bin size for the fluence rate spectrum of $b_E = 1\,\text{keV}$, and a threshold energy of $\delta = 10\,\text{keV}$.

The comparison between the various air-kerma strength values S_K obtained in the different simulations and S_K^{ref} was carried out in terms of the absolute difference $\Delta = |S_K^{ref} - S_K|$, the relative difference $\Delta_S = \Delta/S_K^{ref}$, and the σ-weighted relative difference $\Delta_\sigma = \Delta/\sigma_{ref}$, which gives the number of times that Δ contains the uncertainty of the reference value σ_{ref} and allows us to estimate the significance of the effects under investigation.

3. Results

Table 2 includes a first group of results in which S_K has been calculated in `mix` and `det` simulations for the two sources, with either $b_E = 1\,\text{keV}$ or $b_E = 10\,\text{keV}$, and when both μ_{tr} and μ_{en} are used.

Table 2. Air-kerma strengths S_K^τ with $\tau \equiv \text{tr}, \text{en}$ found in the simulations for the two sources using $\delta = 10\,\text{keV}$, the `fuldec` value of the two isotopes, and the TG-43U1 dry air composition (see Table 1). Results for the `mix` and `det` simulations and for the two considered fluence bin sizes b_E are given. Uncertainties correspond to a coverage factor $k = 3$. The superscripts label the corresponding simulations according to Table A3. The reference values used in the various comparisons made in this study are shown in bold (both in this table and in the others).

		S_K^τ (U GBq^{-1})			
	b_E	Flexisource		microSelectron	
Simulation	(keV)	$\tau \equiv$ tr	$\tau \equiv$ en	$\tau \equiv$ tr	$\tau \equiv$ en
`mix`	1	**304.9(5)** [ref]	303.7(5) [2a]	**98.95(6)** [ref]	98.87(6) [2a]
	10	305.6(5) [2b]	304.4(5) [2c]	98.47(8) [2b]	98.38(8) [2c]
`det`	1	305.0(4) [2d]	303.8(4) [2e]	98.98(8) [2d]	98.90(8) [2e]
	10	305.9(6) [2f]	304.7(6) [2g]	98.49(8) [2f]	98.41(8) [2g]

Because of the observed effects linked to b_E, we carried out two additional simulations similar to the reference ones but for $b_E = 3\,\text{keV}$ and $b_E = 5\,\text{keV}$ in order to analyze the convergence with this parameter. The obtained results are shown in Table 3.

Table 3. Study of the convergence of the air-kerma strength with b_E for the two sources. The reference simulation results are compared to those obtained in the same scenario when changing b_E from 1 keV to 10 keV. Uncertainties correspond to a coverage factor $k = 3$. The superscripts label the corresponding simulations according to Table A3. The reference values used in the various comparisons made in this study are shown in bold.

	S_K^{tr} (U GBq^{-1})	
b_E (keV)	Flexisource	microSelectron
1	**304.9(5)** [ref]	**98.95(6)** [ref]
3	305.7(5) [3a]	99.01(6) [3a]
5	304.9(5) [3b]	99.03(6) [3b]
10	305.6(5) [2b]	98.47(8) [2b]

Regarding electron effects, the first contribution concerns the β emissions produced in the decay of the ^{60}Co and ^{192}Ir isotopes. To estimate these contributions, the reference results are compared to those obtained in `comphs` simulations of both the ^{192}Ir microSelectron and ^{60}Co Flexisource as well as to the `minphs` simulation of the latter. The results are shown in Table 4. The same table shows the S_K values obtained by imposing a very high absorption energy for electrons and positrons (10 MeV). These simulations ruled out any electron contribution, ensuring that any electron (and where applicable, positron) that might be generated as a secondary particle would be stopped immediately afterwards, allowing its transport to be ignored.

Table 4. Air-kerma strengths S_K^{tr} found in `mix` simulations for the two sources, using $\delta = 10\,\text{keV}$, $b_E = 1\,\text{keV}$, and the TG-43U1 dry air composition (see Table 1). Results assuming `fuldec`, `comphs`, and in case of the Flexisource, `minphs` are given. Uncertainties correspond to a coverage factor $k = 3$. The superscripts label the corresponding simulations according to Table A3. The reference values used in the various comparisons made in this study are shown in bold.

Source		S_K^{tr} (U GBq^{-1})	
Spectrum	$E_{abs}(e^{\mp})$	Flexisource	microSelectron
`fuldec`	100 eV	**304.9(5)** [ref]	**98.95(6)** [ref]
`comphs`	100 eV	305.1(4) [4a]	98.76(5) [4a]
	10 MeV	305.2(4) [4b]	98.66(5) [4b]
`minphs`	100 eV	304.9(4) [4c]	—
	10 MeV	305.0(4) [4d]	—

A commonly used method for determining the values of S_K is to calculate the fluence rates via Monte Carlo and use the μ_{en}/ρ coefficients provided by NIST, with adequate interpolation at the required energies to perform the numerical calculation in Equation (4) [6,8,10,11]. Table 5 compares the reference S_K^{tr} results (in boldface) with the S_K^{en} obtained by using the μ_{en}/ρ coefficients provided by NIST [19] in either `fuldec` or `comphs` simulations for the two analyzed sources. In addition to the values obtained with $b_E = 1\,\text{keV}$, those found with $b_E = 10\,\text{keV}$ are shown in order to check whether the interpolation induces some additional effect.

Table 5. Air-kerma strengths S_K^τ found in `mix` simulations for the investigated two sources, using $\delta = 10$ keV and the TG-43U1 dry air composition (see Table 1). Reference results obtained assuming the `fuldec` and μ_{tr}/ρ coefficients used in the PENELOPE calculations are compared to those found with the μ_{en}/ρ taken from the NIST database [19] and assuming both `fuldec` and `comphs`. Results calculated for the two fluence bin sizes of $b_E = 1$ keV and 10 keV, are shown. Uncertainties correspond to a coverage factor $k = 3$. The superscripts label the corresponding simulations according to Table A3. The reference values used in the various comparisons made in this study are shown in bold.

Source Spectrum		b_E **(keV)**	S_K^τ **(U GBq^{-1})**	
			Flexisource	**microSelectron**
`fuldec`	$\tau \equiv$ tr (PENELOPE)	1	**304.9(5)** [ref]	**98.95(6)** [ref]
		10	305.6(5) [2b]	98.47(8) [2b]
	$\tau \equiv$ en (NIST)	1	304.4(2) [5a]	98.94(5) [5a]
		10	304.7(3) [5b]	98.43(7) [5b]
`comphs`	$\tau \equiv$ en (NIST)	1	304.6(1) [5c]	98.74(4) [5c]
		10	304.9(3) [5d]	98.23(11) [5d]

Air composition may also induce some effects on the calculated air-kerma strength. In this respect, it is worth pointing out that in TG-43 [1] it is recommended to use 40% moist air. Air compositions for 40% moist air and dry air included in the PENELOPE database are shown in Table 1. The reference S_K^{tr} values have been calculated again using the μ_{tr}/ρ coefficients determined with the PENELOPE code `MUTREN` for these two new air compositions. The results are shown in Table 6.

Table 6. Air-kerma strengths S_K^{tr} found in `mix` simulations for the two sources, using $\delta = 10$ keV and `fuldec`. Reference results obtained for TG-43U1 dry air are compared to those found with TG-43U1 40% moist air and PENELOPE dry air (see the respective compositions in Table 1). The μ_{tr}/ρ coefficients used here have been calculated with the PENELOPE code `MUTREN`. Values calculated for the two fluence bin sizes of $b_E = 1$ keV and 10 keV are shown. Uncertainties correspond to a coverage factor $k = 3$. The superscripts label the corresponding simulations according to Table A3. The reference values used in the various comparisons made in this study are shown in bold.

	b_E **(keV)**	S_K^{tr} **(U GBq^{-1})**	
		Flexisource	**microSelectron**
Dry air (TG-43U1)	1	**304.9(5)** [ref]	**98.95(6)** [ref]
	10	305.6(5) [2b]	98.47(8) [2b]
Moist air (40%) (TG-43U1)	1	305.4(5) [6a]	99.04(6) [6a]
	10	306.0(6) [6b]	98.51(9) [6b]
Dry air (PENELOPE)	1	305.3(5) [6c]	99.00(6) [6c]
	10	305.6(6) [6d]	98.47(9) [6d]

Another parameter playing a role in this type of calculations is δ, the threshold used as a lower limit in the calculation of the air-kerma rate defined in Equation (2). Table 7 shows the comparison between the air-kerma strengths calculated with $\delta = 10$ keV (reference values) and those found for $\delta = 5$ keV and $\delta = 0$.

To finish, Figure 3 shows the dependence of the air-kerma rate with the angle θ. The results of the Flexisource (red solid circles) and the microSelectron (green open squares) are shown. To permit comparison between both sources, the values have been normalized as follows:

$$R(\theta) = \frac{\dot{K}_\delta(d = 1\,\text{m}, \theta)}{\dot{K}_\delta(d = 1\,\text{m}, \theta = 90°)}. \quad (5)$$

Table 7. Air-kerma strengths S_K^{tr} found in the reference simulations for the two sources, using `fuldec` and TG-43U1 dry air. Results obtained with $\delta = 10$ keV, 5 keV, and 0 are compared. Uncertainties correspond to a coverage factor $k = 3$. The superscripts label the corresponding simulations according to Table A3. The reference values used in the various comparisons made in this study are shown in bold.

	S_K^{tr} (U GBq^{-1})	
δ (keV)	Flexisource	microSelectron
10	**304.9(5)** [ref]	**98.95(6)** [ref]
5	305.0(5) [7a]	99.05(6) [7a]
0	305.0(5) [7b]	99.06(6) [7b]

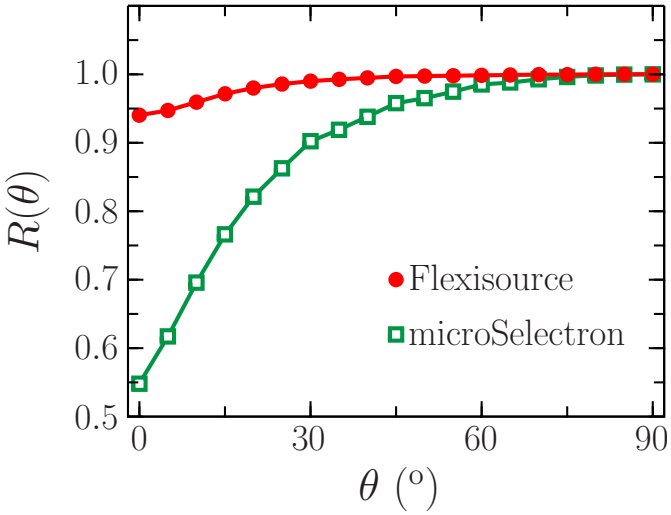


Figure 3. Normalized air-kerma rates as defined in Equation (5) as a function of the angle θ for the Flexisource (red solid circles) and microSelectron (green open squares). Results were obtained in reference simulations using $\delta = 10$ keV, the TG-43U1 dry air composition, `fuldec`, and the μ_{tr}/ρ PENELOPE coefficients. Uncertainties (with coverage factor $k = 3$) are smaller than the symbols used.

4. Discussion

In this study, the values obtained in the reference simulations and used for comparisons with those from other simulations were $S_K^{tr} = 304.9(5)$ U GBq^{-1} for the Flexisource and $S_K^{tr} = 98.95(6)$ U GBq^{-1} for the microSelectron. These values are marked in bold in the tables of the previous section.

4.1. Role of b_E, μ_{tr} Versus μ_{en}, and Detailed vs. Mixed Simulations

The first point to be analyzed concerns the effect of using μ_{en}/ρ instead of μ_{tr}/ρ when calculating the air-kerma rate. As shown in Table 2, in the case of the Flexisource, this change results in a reduction in S_K of $\Delta = 1.2$ U GBq^{-1}, that is, a relative reduction of $\Delta_S = 0.39\%$, while for the microSelectron it is much smaller, amounting to $\Delta = 0.08$ U GBq^{-1}, a relative reduction of $\Delta_S = 0.08\%$. These differences correspond to $\Delta_\sigma = 7.9$ for the Flexisource and $\Delta_\sigma = 3.9$ for the microSelectron.

The different behaviors observed for the two sources can be explained by looking at Figure 4, where the staggered lines show the accumulated air-kerma rate for the two sources in the reference condition,

$$\dot{K}_0^{ref}(\epsilon) = \int_0^\epsilon dE \, \frac{\mu_{tr}(E)}{\rho} \, E \, \dot{\Phi}_E^{ref}, \quad (6)$$

while the blue curve corresponds to the relative difference between both mass coefficients:

$$\kappa_\mu = \frac{\mu_{\rm tr}/\rho - \mu_{\rm en}/\rho}{\mu_{\rm tr}/\rho}. \quad (7)$$

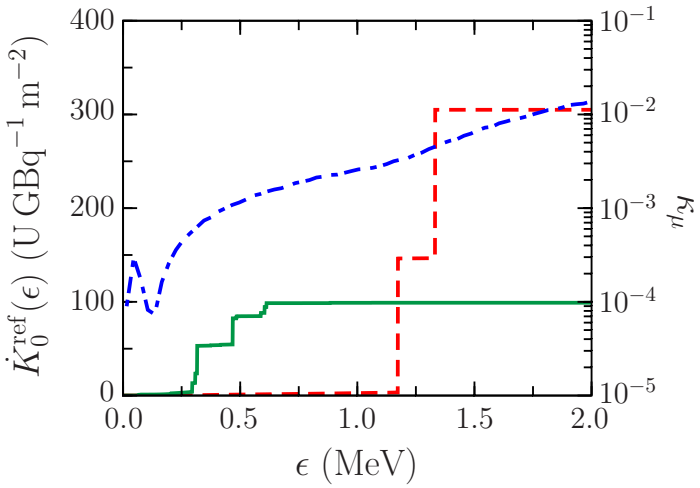


Figure 4. Accumulated $\dot{K}_0^{\rm ref}$ as defined in Equation (6) for the Flexisource (red dashed line) and microSelectron (green solid line), with scale on the left y-axis and relative difference between mass coefficients κ_μ defined as in Equation (7), plotted with the blue dashed-dotted curve and with the scale on the right y-axis.

As can be seen, the difference between $\mu_{\rm en}/\rho$ and $\mu_{\rm tr}/\rho$ becomes greater as the energy of the photons increases, reaching about 1% for $\epsilon = 2$ MeV. On the other hand, the photon energies that contribute significantly to $\dot{K}_0^{\rm ref}$ in the case of the ^{60}Co Flexisource (see red dashed line) are much higher than those for the ^{192}Ir microSelectron (green solid line). Consequently, the ^{60}Co source is about five times more sensitive to the use of $\mu_{\rm en}/\rho$ instead of $\mu_{\rm tr}/\rho$, and the reduction in S_K produced by this change is more evident in the case of the former.

In any case, it is important to note that the difference observed when using $\mu_{\rm en}/\rho$ instead of $\mu_{\rm tr}/\rho$ results in significantly reduced S_K for both sources.

The second aspect to be analyzed is linked to the fluence bin size b_E. In Table 2, the results of the reference mixed calculation, which correspond to $b_E = 1$ keV, are compared to those found using $b_E = 10$ keV (see first two rows). When considering this last bin size, $S_K^{\rm tr}$ increases by $\Delta_S = 0.22\%$ ($\Delta_\sigma = 4.4$) for the Flexisource; however, in the case of the microSelectron it decreases by $\Delta_S = 0.49\%$ ($\Delta_\sigma = 23.6$).

The variations are again significant for both sources, particularly for the latter, where the complex photon spectrum interferes with the b_E value to produce the observed behavior. In fact, the spectrum of the photons reaching the detection sphere in the case of ^{60}Co is dominated by two lines at 1173.23 keV and 1332.49 keV, which are separated by more than 150 keV and situated in a region where the product $E\,\mu_{\rm tr}(E)/\rho$ (entering in Equation (2), which defines the air-kerma rate) varies slowly and smoothly. In this situation, substituting the energy of the emission line by the central energy of a bin with a width of 10 keV instead of 1 keV only introduces a certain uncertainty to the calculation.

The spectrum of ^{192}Ir, on the other hand, consists of several dozens of lines spread from 7.8 keV to about 1.4 MeV, with the bulk of the emission concentrated between 295 keV and 613 keV and an additional intense group of X-rays characteristic of Pt and Os between 61 keV and 78 keV. Below about 100 keV, the product $E\,\mu_{\rm tr}(E)/\rho$ for the air changes rapidly with the energy, so that grouping lines for which the $\mu_{\rm tr}/\rho$ values differ appreciably into a single 10 keV interval and evaluating the coefficient at the center of the interval results in a much larger uncertainty. As a result of this, the air-kerma strength for the Flexisource increases when $b_E = 10$ keV is used instead of $b_E = 1$ keV, with $\Delta_S = 0.22\%$, while for the

microSelectron a reduction is observed with $\Delta_S = 0.49\%$. The sign of the effect is opposite for the two sources, which is simply due to the local curvature of $E\,\mu_{tr}(E)/\rho$ in the regions where the respective spectra are concentrated.

It must be pointed out again that the effect is significant for both sources, though it is much larger in case of the microSelectron than the Flexisource. To analyze the role played by b_E in more detail, two additional simulations, similar to the reference ones but for $b_E = 3$ keV and $b_E = 5$ keV, were carried out; the results obtained for these simulations are compared with those for the previous ones in Table 3. In the case of the Flexisource, the values of S_K^{tr} appear to be stabilized when b_E reduces from 10 keV to 1 keV. For the microSelectron, the difference discussed above between the results obtained with $b_E = 1$ keV and $b_E = 10$ keV is largely reduced when $b_E = 5$ keV, and even more when $b_E = 3$ keV, showing a clear convergence. To reduce b_E below 1 keV would incur a high computational cost; an appropriate compromise between accuracy and calculation time would be to use fluence bins with size $b_E = 1$ keV for ^{192}Ir sources. In any case, it is mandatory to indicate the bin size employed in the simulations when quoting S_K values.

We also analyzed the variations in S_K resulting from running detailed simulations (see second data group in Table 2) instead of the mixed reference simulations. The S_K results slightly increased in `det` simulations, with the largest variation occurring in the case of the Flexisource with $b_E = 10$ keV, where the obtained S_K `det` value was larger than that in the `mix` simulation with $\Delta_S = 0.10\%$, although the two results agreed within 1.7σ. These results indicate that mixed simulations permit a correct calculation of the air-kerma strength.

It is worth pointing out that the same effects observed for the reference results due to the use of μ_{en}/ρ instead of μ_{tr}/ρ are seen in the other cases analyzed, namely, the `mix` simulations with $b_E = 10$ keV and the detailed simulations with the two b_E values considered. The same effect observed for the `mix` simulations when using $b_E = 10$ keV instead of $b_E = 1$ keV is also seen for the `det` simulations.

4.2. Electron Effects

Table 4 shows the comparisons carried out to estimate the effects due to electrons. Considering the complete photon spectra of the isotopes (`comphs`), as recommended in the HEBD-WG report [4], instead of the full decay schemes (`fuldec`) produced a slight increase in the air-kerma strength in the case of the Flexisource ($\Delta_S = 0.07\%$; $\Delta_\sigma = 1.3$), while S_K^{tr} was reduced by $\Delta_S = 0.19\%$ ($\Delta_\sigma = 9.3$) for the microSelectron. Again, different behavior is observed between the two sources. Since the variations produced in the two sources are almost the same in absolute value, at $\Delta = 0.20$ U GBq^{-1} and $\Delta = 0.19$ U GBq^{-1}, the fact that the uncertainties are much smaller for the microSelectron than the Flexisource makes the difference significant for the former but not the latter. Thus, the electron contributions associated with β decay are not relevant for the Flexisource.

The results obtained when electron contributions are fully ruled out (see Table 4 for $E_{abs}(e^{\mp}) = 10$ MeV) indicate that, in case of `comphs`, S_K^{tr} increased by $\Delta_S = 0.10\%$ ($\Delta_\sigma = 2.0$) for the Flexisource and fell by $\Delta_S = 0.29\%$ ($\Delta_\sigma = 14.1$) for the microSelectron. Again, electron effects are more relevant in the case of the microSelectron source, showing up as almost negligible for the Flexisource.

When referring to `minphs` simulations carried out for the ^{60}Co Flexisource (the last data block in Table 4), it can be seen that they produced the same S_K^{tr} value as the reference simulation when $E_{abs}(e^{\mp}) = 100$ eV was considered. However, if electrons were completely stopped by using $E_{abs}(e^{\mp}) = 10$ MeV, $\Delta_S = 0.03\%$ ($\Delta_\sigma = 0.7$), which also agrees with the reference value within the uncertainty. Finally, it is worth noting that the consideration of the minimum photon spectrum instead of the complete spectrum did not produce significant effects, with $\Delta_S = 0.07\%$ ($\Delta_\sigma = 1.4$).

According to these results, it can be stated that electrons may modify S_K through the bremsstrahlung photons and the characteristic X-rays that they can emit while traveling either inside the source active core, in the capsule, or in the cable. In our calculations, it is observed that taking electrons into account reduces S_K for the Flexisource and increases it for the microSelectron, to a greater extent in the latter case.

This may seem surprising, since the magnitude of this indirect contribution is expected to increase with the energy of the electrons, and according to [22] the Q_β value for ^{60}Co (2823.07 keV) is approximately twice that of ^{192}Ir (1459.7 keV). However, the excited state of ^{60}Ni that is most likely populated following the decay of ^{60}Co has a high excitation energy (2505.75 keV); consequently, the electrons emitted by ^{60}Co in that transition have a maximum energy of 317.32 keV, with an average energy of only 95.6 keV. On the other hand, the β decay of ^{192}Ir primarily populates two excited states of ^{192}Pt, with excitation energies of 784.58 keV and 920.92 keV, and the electrons emitted in these transitions have maximum energies of 675.1 keV and 538.8 keV and average energies of 209.9 keV and 162.1 keV, respectively. Since the energies of the electrons emitted during β decay of ^{192}Ir are on average higher than those of the electrons emitted from β decay of ^{60}Co, the former produce more radiation photons in their interactions with the source material and its encapsulation, which then result in a relatively more significant effect on S_K.

Neglecting the β^- emission spectrum along with the transport of photons that it may produce results in a significant variation in the calculation of S_K, and this variation is relatively greater in the case of ^{192}Ir sources.

4.3. Other Calculations

In the case of the Flexisource, the use of the NIST mass energy absorption coefficients (see Table 5) produced a significant reduction of S_K, with $\Delta_S = 0.18\%$ ($\Delta_\sigma = 3.5$). However, this same reduction is almost negligible for the microSelectron ($\Delta_S = 0.01\%$; $\Delta_\sigma = 0.6$). It is worth noting that the differences observed when using the PENELOPE μ_{en}/ρ coefficients (see above) were larger, being significant even in the case of the microSelectron. On the other hand, when considering `comphs` simulations instead of `fuldec`, these differences were reduced for the Flexisource ($\Delta_S = 0.11\%$; $\Delta_\sigma = 2.1$) and increased significantly for the microSelectron, where $\Delta_S = 0.21\%$ ($\Delta_\sigma = 10.3$). Finally, utilizing $b_E = 10$ keV instead of $b_E = 1$ keV introduced larger differences between the corresponding S_K values except in this latter case, for which $\Delta_S = 0.24\%$ and $\Delta_\sigma = 8.5$ were obtained.

Regarding the effects related to the composition chosen for the air in the simulations, Table 6 shows that moist air increased S_K^{tr} by $\Delta_S = 0.16\%$ ($\Delta_\sigma = 3.2$) in the case of Flexisource and by $\Delta_S = 0.09\%$ ($\Delta_\sigma = 4.3$) in the case of microSelectron, and the corresponding results did not agree within 3σ uncertainty. If PENELOPE dry air is considered, the obtained S_K^{tr} agrees with the reference value, with the relative differences being $\Delta_S = 0.13\%$ ($\Delta_\sigma = 2.5$) and $\Delta_S = 0.05\%$ ($\Delta_\sigma = 2.2$) for the Flexisource and microSelectron, respectively.

The effects due to considering a larger fluence bin size in the case of the two new air compositions were similar to those observed for the reference TG-43U1 dry air composition, though it is again worth noting the significant reduction in the air-kerma strength that this bin size produced in the case of the microSelectron source, with $\Delta_\sigma > 20.0$.

The role of the air composition deserves comment. The original TG-43 protocol [1] recommended considering moist air with a 40% degree of humidity. This recommendation was initially maintained in the protocol revision TG-43U1 [2], but was changed to dry air in the HEBD-WG report [3,4]. The difference in the value of S_K between both air compositions is significant, with $\Delta_\sigma > 3$ for both sources.

When referring to the δ parameter (the threshold used to calculate the air-kerma rate; see Equation (2)), the Flexisource and microSelectron again showed very different behavior.

As seen in Table 7, in the former the three calculations carried out with $\delta = 10$ keV (reference values), $\delta = 5$ keV, and $\delta = 0$ agreed within 1σ, with differences $\Delta_S \leq 0.03\%$. This was expected, because as seen in Figure 2 (as well as in Tables A1 and A2), the photon spectrum recommended for ^{60}Co only includes photons with energies above 300 keV.

In case of the microSelectron, going from $\delta = 10$ keV to $\delta = 5$ keV increased S_K by 0.10%, while reducing the threshold even more to $\delta = 0$ added only 0.01%; the S_K^{tr} obtained with these latter two values agreed to within 1σ. In other words, almost the entire effect comes from the 5–10 keV range, which contains precisely the characteristic X-rays of the L-shell of Os and Pt—the daughter elements of ^{192}Ir (7.8–10.0 keV)—and of the K-shell of the elements that constitute the AISI encapsulation of the sources (5.4 keV for Cr, 6.4 keV for Fe, and 7.5 keV for Ni). The latter are produced in much greater abundance by the ^{192}Ir source, the spectrum of which induces a photoelectric component larger than that of ^{60}Co source, in which Compton scattering dominates.

The last point to be analyzed concerns the angular dependence of the air-kerma rate, shown in Figure 3. It is evident that the microSelectron (green open squares) shows a much larger angular dependence than the Flexisource (red solid circles). This behavior had been already pointed out in previous works for the ^{60}Co BEBIG Co0.A86 source [9], for the Flexisource itself [7,16], and also in a comparison between HDR sources of ^{60}Co and ^{192}Ir carried out by Gebremariam et al. [21].

In general, photons emitted from a given point in the active core and moving in the transverse direction with $\theta = 90°$ travel shorter distances through the various materials that compose the sources than those emitted from the same point but traveling at a different polar angle. This means that the probability of self-absorption in the source increases as θ decreases from 90°; in other words, R is expected to increase with θ, as is observed in Figure 3.

As can be seen in Figure 1, the geometric dimensions of the two sources are very similar, and the encapsulation materials are the same; therefore, the distances traveled by the photons in the materials of both sources would be very similar if emitted from the same point and at the same angle. Several reasons jointly explain why $R(\theta)$ is smaller in ^{192}Ir than in ^{60}Co. First, as shown in Figure 2 and in Tables A1 and A2, the energies of the main photon emissions in ^{192}Ir (between 300 and 500 keV) are much lower than those of ^{60}Co (more than 1 MeV); second, the density of Ir is 2.5 times larger than that of Co; third, $Z = 77$ for the former and $Z = 27$ for the latter. Consequently, the attenuation coefficients, which decrease with photon energy and increase with atomic number Z and the density of the material, are much lower in the case of ^{60}Co, which explains the higher values of $R(\theta)$ for this isotope in comparison to ^{192}Ir.

4.4. Comparison with Previous Calculations

It is worth comparing the air-kerma strength obtained in this work with those from previous studies on the same sources analyzed here and on other sources similar to them.

For the Flexisource, Almansa et al. [7] obtained $S_K = 305.1(3)$ U GBq^{-1} in a calculation performed with PENELOPE-2014, using the complete photon spectrum of ^{60}Co without electron transport, with fluence bins of 1 keV, an absorption energy for photons of 10 keV, and the μ_{tr}/ρ coefficients obtained with `MUTREN`. The value obtained in the present work under the same conditions produced a value of 305.2(4) U GBq^{-1} (see Table 4, second data block, $E_{\text{abs}}(e^{\mp}) = 10$ MeV). Both values agree within the uncertainties, differing by only 0.03 %.

Furthermore, when using μ_{en}/ρ instead of μ_{tr}/ρ, Almansa et al. [7] observed a 0.39 % reduction in air-kerma strength, the same decrease that we obtained in our calculations (see Table 2), even though both studies used two different versions of the code published more than a decade apart.

Another ^{60}Co source different to the Flexisource is the BEBIG Co0.A86 source (Eckert & Ziegler BEBIG GmbH, Berlin, Germany). For this source, Guerrero et al. [9],

in a simulation similar to that described just above, reported $S_K = 304.6(7)$ U GBq^{-1}, which is again compatible with the values we obtained for the Flexisource. The main reason for this is that S_K is essentially determined by the isotope emission spectrum, while it is only slightly sensitive to the encapsulation details that, in any case, are rather similar in both sources.

It is also possible to find several studies on the microSelectron in the literature. For a model with a geometry slightly different from that studied in this work, Borg and Rogers [8] reported a value of $S_K = 97.3(1)$ U GBq^{-1} using EGS4, while Berenguer Serrano et al. [23] obtained a value of $S_K = 98.2(3)$ U GBq^{-1} using Geant4. More recently, Almansa et al. [6] obtained $S_K = 98.6(2)$ U GBq^{-1}. In the latter case, the simulation was performed using PENELOPE-2008 and considering the same geometry shown in Figure 1. In our case, $S_K = 98.95(6)$ U GBq^{-1}, which represents a difference of 0.35% compared to the result by Almansa et al., although both agree within a margin of 1.7σ. Tsuji et al. [24] obtained $S_K = 98.29(20)$ U GBq^{-1} in simulations performed with the EGS5 Monte Carlo code, a value from which our result differs significantly.

5. Conclusions

In this work, a systematic analysis of the various quantities contributing to the air-kerma strength defined in the TG-43 protocol has been carried out by using the Monte Carlo code PENELOPE. Simulations are performed for two high-energy HDR brachytherapy sources, Flexisource and microSelectron. To the best of our knowledge, this is the most exhaustive analysis concerning the calculation of the TG-43 air-kerma strength carried out to date. Perhaps the most striking feature of the results obtained here is that the two sources responded very differently to the various calculation scenarios we analyzed.

The overall contribution of electrons to S_K is small, but not negligible. The effect is greater for the ^{192}Ir source. The reason for this is that the dominant β^- branch of ^{60}Co delivers electrons with an average energy of only 95.6 keV, whereas the electrons emitted in the β decay of ^{192}Ir have average energies of 162.1 keV and 209.9 keV.

Mixed and fully detailed electron transport models provide air-kerma strengths that agree within 1.7σ. The mixed simulations, which are much less computationally expensive, are suitable for this type of calculation.

When calculating the air-kerma rate, replacing the mass energy transfer coefficient with the mass energy absorption coefficient is not recommended for any source.

The size of the energy bins used to score photon fluences is the most influential factor among those analyzed in the case of microSelectron; intervals of 1 keV or less are recommended, especially for sources with complex photon spectra.

The (moist or dry) air composition and the value chosen for the photon energy cutoff threshold δ also produce significant effects on the air-kerma strength calculation.

None of the contributions analyzed here alters the reference S_K^{tr} by more than 0.5% when considered individually; however, they are all systematic rather than random, do not have the same sign for the two sources, and their combined effect could be on the order of 1%. Thus, it should be noted that since S_K normalizes the entire TG-43U1 dataset through the dose-rate constant, $\Lambda = \dot{D}(r_0, \theta_0)/S_K$, any relative bias in the Monte Carlo determination of S_K would be propagated to any dose calculated within this protocol. Furthermore, it must be taken into account that a 1% uncertainty is not negligible when compared to the expected accuracy in radiotherapy dosimetry (2–3%) or the uncertainties of the protocol parameters.

The results obtained in this work point out that any Monte Carlo estimation of the air-kerma strength must be carried out with a careful choice of the value of δ, the fluence bin size b_E, and the air composition, using a consistent set of mass coefficients and justifying whether μ_{tr}/ρ or μ_{en}/ρ are employed, and without neglecting to include the emitted electrons or,

of course, their transport. In addition, it is recommended that these values be explicitly stated along with any Monte Carlo estimates of the air-kerma strength so that meaningful comparisons can be made between the various calculations.

Finally, it should be noted that although only two high-energy HDR sources were studied in the present work, in the case of low-energy sources such as those based on ^{125}I or ^{103}Pd, for which $\delta = 5$ keV is typically chosen and for which the fluence is concentrated in the energy region where μ_{tr}/ρ varies most rapidly, the sensitivity with respect to b_E, δ, and the chosen set of mass coefficients is expected to be as large as that observed here or even higher.

Author Contributions: Conceptualization, R.G., J.F.A., and A.M.L.; methodology, R.G., J.F.A., and A.M.L.; software, R.G., J.F.A., and A.M.L.; validation, R.G., J.F.A., and A.M.L.; formal analysis, R.G., J.F.A., and A.M.L.; investigation, R.G., J.F.A., and A.M.L.; resources, R.G., J.F.A., and A.M.L.; data curation, R.G., J.F.A., and A.M.L.; writing—original draft preparation, R.G., J.F.A., and A.M.L.; writing—review and editing, R.G., J.F.A., and A.M.L.; visualization, R.G., J.F.A., and A.M.L.; supervision, R.G., J.F.A., and A.M.L.; project administration, A.M.L.; funding acquisition, A.M.L. All authors have read and agreed to the published version of the manuscript.

Funding: This work has been partially funded by the Spanish Ministerio de Ciencia y Competitividad (PID2022-137543NB-I00), the European Regional Development Fund (ERDF), and the Junta de Andalucía (FQM387).

Institutional Review Board Statement: Not applicable.

Informed Consent Statement: Not applicable.

Data Availability Statement: Data are available on request.

Conflicts of Interest: The authors declare no conflicts of interest.

Abbreviations

The following abbreviations are used in this manuscript:

`comphs`	Complete photon spectrum
`det`	Detailed
`fuldec`	Full decay scheme
HDR	High dose rate
kerma	Kinetic energy released per unit mass
`minphs`	Minimum photon spectrum
`mix`	Mixed

Appendix A

The photon spectra used in the simulations are plotted in Figure 2.

The energy E and intensity I of the ^{60}Co photon emissions considered in `comphs` simulations of the Flexisource are listed in Table A1. These emissions are those recommended in the HEBD-WG report [4]. The `minphs` simulations were carried out by considering only the two emissions marked in boldface.

Table A1. Photon spectrum of ^{60}Co used in the Flexisource simulations. The two emissions marked in boldface are those used in case of the `minphs` simulations.

E (keV)	I (%)	E (keV)	I (%)	E (keV)	I (%)
347.14	0.0075	826.10	0.0076	**1173.23**	**99.85**
1332.49	**99.9826**	2158.57	0.0012	2505.69	2×10^{-6}

In the case of the `comphs` simulations for the microSelectron, the photon spectrum considered for ^{192}Ir included the emissions shown in Table A2.

Table A2. Photon spectrum of ^{192}Ir used in the microSelectron simulations.

E (keV)	I (%)	E (keV)	I (%)	E (keV)	I (%)
7.822	0.028	8.266	0.076	8.840	0.064
8.911	0.57	9.337	0.0087	9.362	0.166
9.443	1.47	9.975	0.0271	10.176	0.042
10.217	0.0078	10.354	0.408	10.511	0.058
10.590	0.133	10.840	0.0211	10.854	0.056
10.871	0.0075	11.071	1.24	11.235	0.073
11.242	0.354	11.562	0.0292	12.096	0.079
12.385	0.0066	12.422	0.0133	12.500	0.019
12.942	0.245	13.271	0.030	13.273	0.018
13.361	0.025	60.903	0.00106	61.486	1.20
63.000	2.07	64.514	0.00286	65.122	2.65
66.831	4.53	71.079	0.239	71.414	0.460
71.875	0.0113	73.363	0.162	73.590	0.0188
75.368	0.533	75.749	1.029	76.233	0.0265
77.831	0.365	78.073	0.0478	110.093	0.0126
136.34348	0.183	176.98	0.0043	201.3112	0.472
205.79549	3.300	280.04	0.023	283.2668	0.262
295.95827	28.67	308.45692	30.00	316.50791	82.81
329.312	0.0185	374.4852	0.721	416.4714	0.664
420.532	0.0737	468.07152	47.83	484.5780	3.184
485.30	0.0022	489.039	0.443	588.5845	4.515
593.37	0.0426	599.35	0.0039	604.41464	8.23
612.46564	5.309	703.98	0.0053	765.8	0.00149
884.5418	0.2923	1061.48	0.0528	1089.7	0.00108
1378.3	0.00124				

Table A3 summarizes the characteristics of the various simulations carried out in the present work.

Table A3. Characteristics of the simulations carried out in the present work. The first row corresponds to the reference simulation. The labels in the first column identify the various simulations and have been used in the various tables throughout the text; in these labels the number indicates the table in which the corresponding results are shown. In the last column, "dry (TG)", "moist (TG)", and "dry (PEN)" refer to the dry and moist (40%) air compositions quoted in the TG-43U1 and the dry air composition taken from the PENELOPE database (see Table 1). In all simulations, the absorption energy for photons was $E_{\mathrm{abs}}(\gamma) = 1$ keV in all the materials included in the geometry. The gray cells show the changes of the corresponding simulation with respect to that of the reference.

	Simulation	Source Spectrum	μ_τ	$(\mu_{\mathrm{tr}}, \mu_{\mathrm{en}})$ Database	$E_{\mathrm{abs}}(e^{\mp})$ (eV)	b_E (keV)	δ (keV)	Air Composition
[ref]	`mix`	`fuldec`	μ_{tr}	PENELOPE	10^2	1	10	dry (TG)
[2a]	`mix`	`fuldec`	μ_{en}	PENELOPE	10^2	1	10	dry (TG)
[2b]	`mix`	`fuldec`	μ_{tr}	PENELOPE	10^2	10	10	dry (TG)
[2c]	`mix`	`fuldec`	μ_{en}	PENELOPE	10^2	10	10	dry (TG)
[2d]	`det`	`fuldec`	μ_{tr}	PENELOPE	10^2	1	10	dry (TG)
[2e]	`det`	`fuldec`	μ_{en}	PENELOPE	10^2	1	10	dry (TG)
[2f]	`det`	`fuldec`	μ_{tr}	PENELOPE	10^2	10	10	dry (TG)
[2g]	`det`	`fuldec`	μ_{en}	PENELOPE	10^2	10	10	dry (TG)
[3a]	`mix`	`fuldec`	μ_{tr}	PENELOPE	10^2	3	10	dry (TG)
[3b]	`mix`	`fuldec`	μ_{tr}	PENELOPE	10^2	5	10	dry (TG)

Table A3. *Cont.*

	Simulation	Source Spectrum	μ_τ	(μ_{tr}, μ_{en}) Database	$E_{abs}(e^{\mp})$ (eV)	b_E (keV)	δ (keV)	Air Composition
[4a]	mix	comphs	μ_{tr}	PENELOPE	10^2	1	10	dry (TG)
[4b]	mix	comphs	μ_{tr}	PENELOPE	10^7	1	10	dry (TG)
[4c]	mix	minphs	μ_{tr}	PENELOPE	10^2	1	10	dry (TG)
[4d]	mix	minphs	μ_{tr}	PENELOPE	10^7	1	10	dry (TG)
[5a]	mix	fuldec	μ_{en}	NIST	10^2	1	10	dry (TG)
[5b]	mix	fuldec	μ_{en}	NIST	10^2	10	10	dry (TG)
[5c]	mix	comphs	μ_{en}	NIST	10^2	1	10	dry (TG)
[5d]	mix	comphs	μ_{en}	NIST	10^2	10	10	dry (TG)
[6a]	mix	fuldec	μ_{tr}	PENELOPE	10^2	1	10	moist (TG)
[6b]	mix	fuldec	μ_{tr}	PENELOPE	10^2	10	10	moist (TG)
[6c]	mix	fuldec	μ_{tr}	PENELOPE	10^2	1	10	dry (PEN)
[6d]	mix	fuldec	μ_{tr}	PENELOPE	10^2	10	10	dry (PEN)
[7a]	mix	fuldec	μ_{tr}	PENELOPE	10^2	1	5	dry (TG)
[7b]	mix	fuldec	μ_{tr}	PENELOPE	10^2	1	0	dry (TG)

References

1. Nath, R.; Anderson, L.L.; Luxton, G.; Weaver, K.A.; Williamson, J.F.; Meigooni, A.S. Dosimetry of interstitial brachytherapy sources: Recommendations of the AAPM Radiation Therapy Committee Task Group No. 43. *Med. Phys.* **1995**, *22*, 209–234. [CrossRef] [PubMed]
2. Rivard, M.J.; Coursey, B.M.; DeWerd, L.A.; Hanson, W.F.; Huq, M.S.; Ibbott, G.S.; Mitch, M.G.; Nath, R.; Williamson, J.F. Update of the AAPM Task Group No. 43 Report: A revised AAPM protocol for brachytherapy dose calculations. *Med. Phys.* **2004**, *31*, 633–674. Erratum in *Med. Phys.* **2004**, *31*, 3532–3533. [CrossRef] [PubMed]
3. Pérez-Calatayud, J.; Ballester, F.; Das, R.K.; DeWerd, L.A.; Ibbott, G.S.; Meigooni, A.S.; Ouhib, Z.; Rivard, M.J.; Sloboda, R.S.; Williamson, J.F. Dose calculation for photon-emitting brachytherapy sources with average energy higher than 50 keV: Report of the AAPM and ESTRO. *Med. Phys.* **2012**, *39*, 2904–2929. [CrossRef] [PubMed]
4. Pérez-Calatayud, J.; Ballester, F.; Das, R.K.; DeWerd, L.A.; Ibbott, G.S.; Meigooni, A.S.; Ouhib, Z.; Rivard, M.J.; Sloboda, R.S.; Williamson, J.F. *Dose Calculation for Photon-Emitting Brachytherapy Sources with Average Energy Higher Than 50 keV: Full Report of the AAPM and ESTRO*; Report of the High Energy Brachytherapy Source Dosimetry (HEBD) Working Group; American Association of Physicists in Medicine: College Park, MD, USA, 2012. Available online: https://www.aapm.org/pubs/reports/RPT_229_full.pdf (accessed on 13 October 2026).
5. Seltzer, S.M.; Bartlett, D.T.; Burns, D.T.; Dietze, G.; Menzel, H.-G.; Paretzke, H.G.; Wambersie, A.; Tada, J. Fundamental quantities and units for ionizing radiation. ICRU Report No. 85. *J. ICRU* **2011**, *11*, 1–31. [CrossRef] [PubMed]
6. Almansa, J.F.; Torres, J.; Guerrero, R. Monte Carlo dosimetry of the most commonly used ^{192}Ir high dose rate brachytherapy sources. *Rev. Fís. Méd.* **2011**, *12*, 159–168.
7. Almansa, J.F.; Guerrero, R.; Torres, J.; Lallena, A.M. Monte Carlo dosimetric characterization of the Flexisource Co-60 high-dose-rate brachytherapy source using PENELOPE. *Brachytherapy* **2017**, *16*, 1073–1080. [CrossRef] [PubMed]
8. Borg, J.; Rogers, D.W.O. Spectra and air-kerma strength for encapsulated ^{192}Ir sources. *Med. Phys.* **1999**, *26*, 2441–2444. [CrossRef] [PubMed]
9. Guerrero, R.; Almansa, J.F.; Torres, J.; Lallena, A.M. Dosimetric characterization of the ^{60}Co BEBIG Co0.A86 high dose rate brachytherapy source using PENELOPE. *Phys. Med.* **2014**, *30*, 960–967. [CrossRef] [PubMed]
10. Taylor, R.E.P.; Rogers, D.W.O. EGSnrc Monte Carlo calculated dosimetry parameters for ^{192}Ir and ^{169}Yb brachytherapy sources. *Med. Phys.* **2008**, *35*, 4933–4944. [CrossRef] [PubMed]
11. Taylor, R.E.P.; Rogers, D.W.O. An EGSnrc Monte Carlo-calculated database of TG-43 parameters. *Med. Phys.* **2008**, *35*, 4228–4241. [CrossRef] [PubMed]
12. Safigholi, H.; Chamberland, M.J.P.; Taylor, R.E.P.; Martinov, M.P.; Rogers, D.W.O.; Thomson, R.M. Update of the CLRP Monte Carlo TG-43 parameter database for high-energy brachytherapy sources. *Med. Phys.* **2023**, *50*, 1928–1941. [CrossRef] [PubMed]
13. Ballester, F.; Granero, D.; Pérez-Calatayud, J.; Melhus, C.S.; Rivard, M.J. Evaluation of high energy brachytherapy source electronic disequilibrium and dose for emitted electrons. *Med. Phys.* **2009**, *36*, 4250–4256. [CrossRef] [PubMed]

14. Daskalov, G.M.; Löffler, E.; Williamson, J.F. Monte-Carlo aided dosimetry of a new high dose-rate brachytherapy source. *Med. Phys.* **1998**, *25*, 2200–2208. Erratum in *Med. Phys.* **2000**, *27*, 1999. [CrossRef] [PubMed]
15. Granero, D.; Vijande, J.; Ballester, F.; Rivard, M.J. Dosimetry revisited for the HDR 192Ir brachytherapy source model mHDR-v2. *Med. Phys.* **2011**, *38*, 486–494. [CrossRef] [PubMed]
16. Vijande, J.; Granero, D.; Pérez-Calatayud, J.; Ballester, F. Monte Carlo dosimetric study of the Flexisource Co-60 high dose rate source. *J. Cont. Brachytherapy* **2012**, *4*, 34–44. [CrossRef] [PubMed]
17. Baltas, D.; Karaiskos, P.; Papagiannis, P.; Sakelliou, L.; Loeffler, E.; Zamboglou, N. Beta versus gamma dosimetry close to Ir-192 brachytherapy sources. *Med. Phys.* **2001**, *28*, 1875–1882. [CrossRef] [PubMed]
18. Wang, R.; Li, X.A. Dose characterization in the near-source region for two high dose rate brachytherapy sources. *Med. Phys.* **2002**, *29*, 1678–1686. [CrossRef] [PubMed]
19. Hubbell, J.H.; Seltzer, S.M. *Tables of X-Ray Mass Attenuation Coefficients and Mass Energy-Absorption Coefficients from 1 keV to 20 MeV for Elements Z=01 to 92 and 48 Additional Substances of Dosimetric Interest*; National Institute of Standards and Technology: Gaithersburg, USA, 2004. [CrossRef]
20. Salvat, F. PENELOPE-*2024: A Code System for Monte Carlo Simulation of Electron and Photon Transport*; Document NEA/MBDAV/R(2024)1; OECD Nuclear Energy Agency: Barcelona, Spain, 2025.
21. Gebremariam, T.Y.; Geraily, G.; Jassim, H.H.; Gholami, S. Dosimetric comparison between microSelectron iridium-192 and flexi cobalt-60 sources in high-dose-rate brachytherapy using Geant4 Monte Carlo code. *J. Cont. Brachytherapy* **2023**, *15*, 141–147. [CrossRef] [PubMed]
22. Bé, M.-M.; Coursol, N.; Duchemin, B.; Lagoutine, F.; Legrand, J.; Debertin, K.; Schönfeld, E. *Table de Radionucléides. Note Technique LNHB 2011/53*; Laboratoire National Henri Becquerel, CEA: Gif-sur-Yvette, France, 2011. Available online: http://www.lnhb.fr/accueil/donnees-nucleaires/donnees-nucleaires-tableau/ (accessed on 13 October 2026).
23. Berenguer Serrano, R.; Rivera Giménez, M.; Núñez Quintanilla, A.; Gutiérrez Pérez, M. Evaluación de la dosimetría de una fuente de Ir-192 de alta tasa en un medio con dispersión incompleta mediante cálculo de Monte Carlo. *Rev. Fís. Méd.* **2006**, *7*, 107–112.
24. Tsuji, S.; Narihiro, N.; Oita, M.; Namito, Y.; Hirayama, H. High dose rate ^{192}Ir brachytherapy source model Monte Carlo dosimetry: mHDR-v2 and mHDR-v2r. *PLoS ONE* **2024**, *19*, e0298550. [CrossRef] [PubMed]

Disclaimer/Publisher's Note: The statements, opinions and data contained in all publications are solely those of the individual author(s) and contributor(s) and not of MDPI and/or the editor(s). MDPI and/or the editor(s) disclaim responsibility for any injury to people or property resulting from any ideas, methods, instructions or products referred to in the content.